MAGNETO-RHEOLOGICAL TUNED LIQUID COLUMN DAMPERS TO IMPROVE RELIABILITY OF WIND TURBINE TOWERS

Conference Paper · December 2017

4 authors:

Saptarshi Sarkar
Trinity College Dublin

Breiffni Fitzgerald
Trinity College Dublin

Biswajit Basu
Trinity College Dublin

Arunasis Chakraborty
Indian Institute of Technology Guwahati

ICOVP, 13th International Conference on Vibration Problems
29th November – 2nd December, 2017, Indian Institute of Technology Guwahati, INDIA

MAGNETO-RHEOLOGICAL TUNED LIQUID COLUMN DAMPERS TO IMPROVE RELIABILITY OF WIND TURBINE TOWERS

S. SARKAR[PR], B. FITZGERALD[CR], B. BASU

Department of Civil, Structural & Environmental Engineering, Trinity College Dublin, Dublin, Ireland
sarkars@tcd.ie, fitzgeb7@tcd.ie, bbasu@tcd.ie

A. CHAKRABORTY

Department of Civil Engineering, Indian Institute of Technology Guwahati, India
arunasis@iitg.ernet.in

Abstract. The size of wind turbines has increased exponentially since their induction. Modern multi mega-watt wind turbines are highly flexible structures supported by tall slender towers. These towers cost approximately 30% of the complete wind turbine assembly. It becomes very apparent that these towers need to be protected against damage induced by dynamic inflow wind. This paper uses probabilistic tools to assess the improvement of structural reliability when these towers are equipped with Magneto-Rheological Tuned Liquid Column Dampers (MR-TLCDs). A reduced order dynamic system of the wind turbine based on the Lagrangian formulation is coupled with two MR-TLCDs to suppress tower fore-aft and side-to-side vibrations. Multiple aeroelastic simulations are conducted for various full-field inflow wind speeds generated using the TurbSim package distributed by NREL. The magneto-rheological dampers are operated in a semi-active mode under optimal control framework to take advantage of the fact that these fluids can change their property (i.e. shear stress) instantaneously when subjected to a magnetic field. This allows instantaneous modification of damping of the device. This variable damping is used here as a semi-active control input. Response reduction of approximately 30-40% is obtained for side-to-side motion while less reduction is obtained in fore-aft vibrations due to high aerodynamic damping. Multiple limit states are established in this study to assess reliability of the tower. Numerical investigations conducted ascertains the effectiveness of the semi-active controllers to improve structural response and reliability of the wind turbine tower.

Keywords. Semi-active MR-TLCD, Clipped optimal control, MBC transformation, Fragility analysis.

1. Introduction

In a world with increasing demand of economically viable and sustainable sources of energy, wind energy is likely to play a major role in the coming decades. The move towards wind energy has been driven primarily by cost as the wind turbine prices have fallen by almost a third since 2009. When adding new capacity to an existing power grid wind energy has become the cheapest option, and prices continue to fall. According to GWEC 2016 [1] some onshore wind farms are now delivering electricity for as little as 4 US cents per kWh. Nuclear power costs three times more to produce in America than onshore wind. In Europe, the Middle East and Africa GWEC 2015 [2] new coal/gas-fired power plants costs up to 30% more. Due to these huge reductions in the cost of wind energy, the past decade has seen rapid growth and expansion of wind turbines and wind farms worldwide. The Global Wind Energy Council (GWEC) calculated the global total installed capacity for wind power at the end of 2015 as 432.9 GW [2], this represents an increase of over 600% compared to the 2005 figure of 59.1 GW [3]. This exponential increase in installed capacity in only ten years has been made possible due to developments in wind turbine technology and design.

Wind turbines are now the largest rotating machines on Earth. The past decade has seen the size of wind turbine blades and towers increase dramatically. Current state-of-the-art wind turbines have very large, flexible blades and are supported by very tall, slender towers. These components are manufactured from lightweight high-strength materials and therefore are very flexible and lightly damped. Due to their structural characteristics, blades and towers are very susceptible to wind induced vibrations and they may undergo significant vibration during operation under turbulent wind. It has been well known for over a decade that blade vibrations can have a negative impact on power production [4]. Tower vibrations may slow down wind energy conversion to electrical power and reduce the fatigue life of the structure. Dueñas-Osorio and Basu [6] investigated wind turbine unavailability as a function of wind-induced vibration of the tower. Tower vibration can lead to the malfunction of acceleration-sensitive equipment housed in the nacelle of the wind turbine, resulting in reduced annual wind turbine availability [6]. Moreover, a significant number of tower collapses have been attributed to excessive tower vibration during strong wind events [7]. It is clear then, that the flexible components of modern wind turbines are susceptible to vibration issues which may have a significant impact on downtime, lifetime of the components, and even on the overall integrity of the structural system. These impacts will have associated implications for the cost of wind power. Therefore, there is now increasing interest on reducing the harmful effects of structural vibration on wind turbine blades and towers in the wind energy industry.

The wind energy industry is currently applying technologies and techniques developed in the fields of structural control and health monitoring to reduce vibrations in blades and towers. The application of structural control strategies to wind turbines is now a very active area of research. Murtagh *et al.* [8] and Lackner and Rotea [9] investigated the use of a passive tuned mass dampers (TMDs) to reduce tower vibration, Colwell and Basu [5] used a Tuned Liquid Column Damper (TLCD) to reduce vibrations of offshore wind turbine towers. Arrigan *et al.* [11] developed semi-active TMDs to control the vibrations of wind turbine towers and blades. The literature is still somewhat sparse on active control schemes for wind turbine towers and blades, however, there is recent work published in this area. Lackner and Rotea [10], Fitzgerald and Basu [12], and Fitzgerald *et al.* [13] have investigated the use of active structural control techniques with mass dampers for mitigating vibrations in wind turbine blades and towers. Innovative hardware configurations adopting active elements mounted in wind turbine blades and towers have also been proposed by Fitzgerald and Basu [14] and Staino *et al.* [15].

There has been a lot of work done on structural control of wind turbines in recent years, however, literature is not generally available which demonstrates the capability of structural control schemes to improve the reliability of wind turbine components. Improving the structural reliability of wind turbines is a key concern. Mensah and Dueñas-Osorio [16] recently demonstrated that the use of TLCDs in turbine towers can help achieve long-term reliability and risk targets for utility scale wind turbines. Tuned Column Liquid Dampers (TLCDs) are a class of passive dampers which utilize the gravitational restoring force on a column of liquid to mitigate vibrations. They were first introduced by Sakai *et al.* [27]. It is essentially a liquid filled U tube with an orifice in between to provide a certain level of damping in the motion of the liquid. These types of dampers are extremely popular due to its simple design and nominal maintenance. Two TLCDs, each consisting of a four-storey high, 50,000-gallon water tank, were placed at the top of the 46-storey One Wall Centre combined hotel and residential building in Vancouver [29] to protect it from wind induced vibrations. Considerable research has gone into the optimum design of a TLCD in the past few decades. Yalla and Kareem [31] and Wu *et al.* [30] summarises the design parameters of the TLCD for optimum vibration control. Attempts has also been made to actively control the orifice opening ratio to control the damping of the TLCD leading to a semi-active damper. Yalla *et al.* [32] demonstrates one such attempt. But, there has been no practical implementation of a TLCD with variable orifice opening, mainly due the difficulties of implementation. Subsequently, Ni *et al.* [26] and Wang *et al.* [29] proposed the used of magneto-rheological fluid in the TLCD instead of water, and actively controlling the damping of the device by changing the viscosity of the liquid by applying an external magnetic field. Since, this change is instantaneous, the implementation of this device as a semi-active controller was feasible.

In this paper, a flexible wind turbine model is proposed in order to study the dynamics of wind turbine vibrations, including the coupling between the in-plane and the out-of-plane modes of the blade due to the structural pre-twist of the blades. The equations of motion are derived by taking into account the blade-tower interaction. 3D wind fields are used from the TurbSim [17] package which include the effect of shear and turbulence in the wind field. Multiple semi-active MR-TLCDs, under optimal control framework, are proposed in the paper to mitigate vibrations. The two major advantages of MR-TLCD over a traditional TLCD are, firstly, the use of MR fluid brings down the area requirement by 2.5 times and secondly, the yield stress of the MR fluid can be instantaneously controlled which leads to a semi-active controller. In this study, both the advantages are attempted to be utilized. The wind turbine model is used to estimate the fore-aft and side-to-side displacement of the tower in order to assess its reliability. Complete aeroelastic simulations carried out on the model in time domain with and without the semi-active MR-TLCDs. Results indicate that the proposed controller reduces the probability of exceeding a given displacement limit at various wind speeds and thus it improves the reliability of the blade and tower response.

2. Dynamic Model of HAWT

The dynamic model of the horizontal axis wind turbine shown in *Figure 1* is derived based on Lagrangian formulation following the works of [13]. For this purpose, the blades and the tower are idealized by their fundamental mode. A rotating coordinate system is fixed to the rotating blades. The azimuthal angle of the i^{th} blade in a three bladed wind turbine is given as

$$\psi_i = \Omega t + (i-1)\frac{2\pi}{3} \qquad i = 1,2,3 \tag{1}$$

The displacements of the blade in the out-of-plane and in-plane directions can be obtained as

$$u_{i,j} = \phi_j(r) q_i(t) \quad i = 1,2,3; \quad j = 1,2 \tag{2}$$

Where i denotes the blade number and, $j = 1$ denotes the out-of-plane/fore-aft direction and $j = 2$ denotes the in-plane/side-to-side direction. ϕ_j is the fundamental mode shape of the blades in the j^{th} direction and, q_i is the tip displacement of the i^{th} blade. The velocity of a point at a distance r from the hub in the rotating frame is given as

$$\mathbf{v}_{b,i} = (\dot{q}_{4,2}\sin\psi_i - \Omega u_{i,2})\hat{\imath} + (\Omega r + \dot{u}_{i,2} + \dot{q}_{4,2}\cos\psi_2)\hat{\jmath} + (\dot{u}_{i,1} + \dot{q}_{4,1})\hat{k} \qquad (3)$$

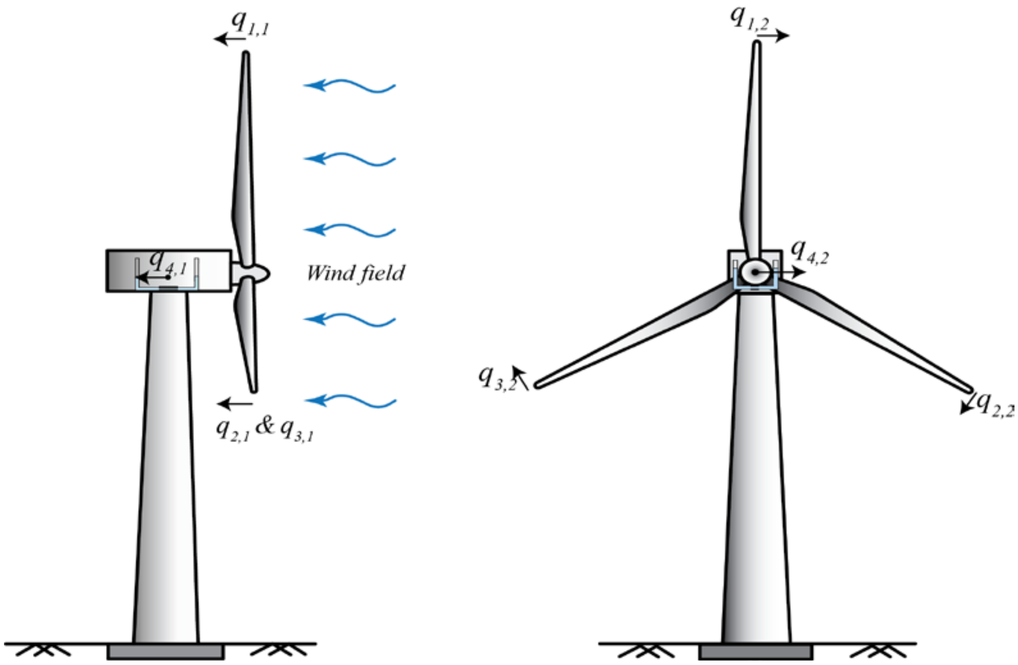

***Figure 1**. Side and front view of HAWT*

To derive the equilibrium equation, principle of conservation of energy can be employed through the Euler-Lagrangian equation that requires the kinetic and potential energy of the system. The kinetic energy is given as

$$T = \frac{1}{2}\sum_{i=1}^{3}\int_0^R \mu(r)|\,\mathbf{v}_{b,i}|^2 dr + \frac{1}{2}\sum_{j=1}^{2} M_o\dot{q}_{4,j}^2 \qquad (4)$$

Where, $\mu(r)$ is the mass density of the blade. M_o is the mass of nacelle and tower assembly. $q_{4,j}$ is the tip displacement of the tower in the j^{th} direction. The potential energy of the system can be written as

$$V = \frac{1}{2}\sum_{i=1}^{3}\sum_{j=1}^{2}\left\{\sum_{k=1}^{2} K_{e,jk}q_{i,j}q_{i,k} + (K_{c,j} + K_{g,j}\cos\psi_i)q_{i,j}^2\right\} + \frac{1}{2}\sum_{j=1}^{2} K_{t,j}q_{4,j}^2 \qquad (5)$$

Where, $K_{e,jk}$ is the elastic stiffness of the blades given as

$$K_{e,jk} = \int_0^R EI_{jk}(r)\phi_j''(r)\phi_k''(r)\,dr \qquad j = 1,2 \qquad (6)$$

The flexural rigidity of the blades are normally provided in literature in the flapwise and edgewise directions. These quantities must be transformed to the out-of-plane and in-plane depending on the structural pre-twist angle. For details on the transformations, refer [13].

$K_{c,j}$, $K_{g,j}$ are the centrifugal and gravitational stiffening/softening of the blades associated with the j^{th} mode of the blade. For details of the expressions, refer [13]. The expressions of kinetic and potential energy of the system can then be substituted in the Euler-Lagrangian equation

$$\frac{d}{dt}\left(\frac{\partial T}{\partial q}\right) - \frac{\partial T}{\partial q} + \frac{\partial V}{\partial q} = f \tag{7}$$

Where, f is the generalized loads, which comprises of generalized aerodynamic load f^a and the generalized gravitational loads f^g. The generalized coordinates are

$$q = [\, q_{1,1} \quad q_{2,1} \quad q_{3,1} \quad q_{4,1} \quad q_{1,2} \quad q_{2,2} \quad q_{3,2} \quad q_{4,2}]^T \tag{8}$$

The equations of motion can be written in matrix form

$$M(t)\ddot{q} + C(t)\dot{q} + K(t)q = f \tag{9}$$

The details of the matrices are provided in the appendix.

2.2 Aerodynamic loads

The aerodynamic loads on the wind turbine is estimated through an unsteady BEM (Blade Element Momentum) model. 3D wind fields are generated using the TurbSim [17] package distributed by NREL. The full field files generate by TurbSim accounts for vertical and horizontal wind shear and spatially coherent turbulent wind. The package can be used to generate full field wind files with varying turbulence intensity levels, power law coefficients for wind shear and characteristic wind speeds at hub height. The unsteady BEM model developed uses this 3D wind field to estimated aerodynamic loads based on quasi-static aerodynamic properties (lift and drag) of the blades. The steady BEM method is widely available in literature [19], [25], [35]. Hansen [19] outlines the unsteady BEM model. The dynamic wake model by Øye [19] is used to account for the time delay before the induced velocities are in equilibrium with the aerodynamic loads. The Blade Element Momentum equations are solved using the approach proposed by Ning [38]. The major change introduced by this approach is rather than solving the two unknowns (i.e. the axial and tangential induction factors) the equations the written so that the only unknown is the inflow angle θ. For this purpose, different equations are used for different solution regions like the momentum, empirical or the propeller brake region. The empirical region is estimated using Glauert's correction with Buhl's modification. Writing different equations for each region allows circumventing the traditional iterative procedure of solving the BEM equations. A residue function (function of inflow angle θ) is formed using the previous value of θ as an initial guess. Root finding methods like that of Brent's is then used to find the final value of θ. Prandtl's hub and tip loss correction factors are also included to account for the vortices generated by the blade tips and the hub. The model is also capable of accounting for skewed inflow using a correction on axial induction factor proposed by Pitt and Peters [35].

For complete aeroelastic simulations, the blade velocities are returned to the BEM model so that the aerodynamic loads are estimated on the relative velocities. In *Figure 2*, V and V' are the downwind and crosswind speeds obtained from TurbSim. $\phi(r)q_{1,i}$ and $\phi(r)q_{2,i}$ are the blade velocities at section r of the i^{th} blade. θ, β, κ and α are the inflow, pitch, structural pre-twist angle and angle of attack of the section respectively. The solution of the BEM equations at each section gives the elemental lift and drag forces. The elemental out-of-plane force (i.e. thrust) and in-plane force (i.e. torque) on the i^{th} blade can be estimated from these forces depending on the inflow angle as

$$p_{i,F}(r,t) = p_{i,l}(r,t)\cos\theta_i(r,t) + p_{i,d}(r,t)\sin\theta_i(r,t) \tag{10}$$

$$p_{i,T}(r,t) = p_{i,l}(r,t)\sin\theta_i(r,t) - p_{i,d}(r,t)\cos\theta_i(r,t) \tag{11}$$

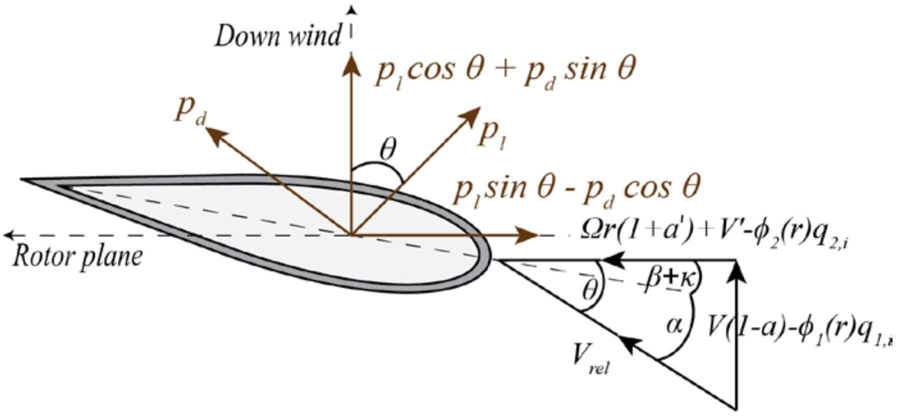

Figure 2. Blade element velocities and forces

The virtual work done by the aerodynamic loads can be given as

$$\delta W^a = \sum_{i=1}^{3}\left(\delta q_{i,1}P_{i,1} + \delta q_{i,2}P_{i,2}\right) + \delta q_{4,1}P_{4,1} + \delta q_{4,2}P_{4,2} \tag{12}$$

Where,

$$P_{i,1} = \int_0^R p_{i,F}\phi_1(r)dr \tag{13}$$

$$P_{i,2} = \int_0^R p_{i,T}\phi_2(r)dr \tag{14}$$

$$P_{4,1} = \sum_{i=1}^{3}\int_0^R p_{i,F}dr \tag{15}$$

$$P_{4,2} = \sum_{i=1}^{3}\int_0^R p_{i,T}dr\cos\psi_i \tag{16}$$

Finally, the aerodynamic loads can be given as

$$f^a = \frac{\partial W^a}{\partial q} \tag{17}$$

2.3 Gravitational loads

The rotational of the blades in the vertical plane creates a sinusoidal load on the blades due to the action of gravity. The in-plane generalized coordinates experience this gravitational load. Since, the blades are made of lightweight glass fiber and carbon fiber, the effect of gravitational load is negligible compared to the aerodynamic loads. For sake of accuracy, this load is also included in the model. The virtual work done by the gravitational force on the blade is

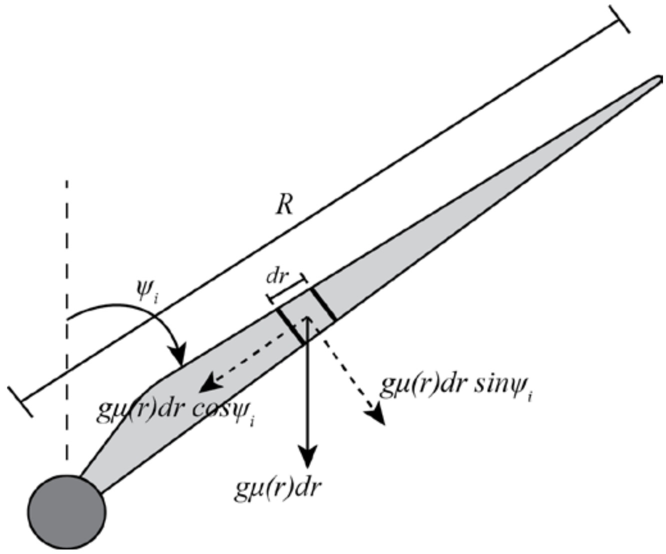

Figure 3. Gravity loads on a blade

$$\delta W^g = \sum_{i=1}^{3} \int_0^R g\mu(r) \sin\psi_i (\delta q_{i,2} \phi_2(r) + \delta q_{4,2} \cos\psi_i) dr \tag{18}$$

Again, the generalized gravitational loads can be obtained as

$$f^g = \frac{\partial W^g}{\partial q} \tag{19}$$

Gravitational load on the nacelle is very small as blades are 120° apart and the horizontal components cancel each other. Hence, it can be neglected without loss of accuracy.

3. Dynamic Model of HAWT-MR-TLCD Coupled System

The MR-TLCD is a U tube filled with MR fluid as shown in *Figure 4(b)*. The density of the liquid is denoted by ρ_l and it has two fixed poles at the middle of the horizontal leg. The damping term of a MR-TLCD is the combination of dissipative force due to the head loss and the strength of magnetic field, which modifies the viscosity of the fluid. This leads to non-linear damping coefficient. In various stochastic and frequency domain studies statistical linearization is often used to obtain an equivalent damping ratio. This is carried out either as an iterative procedure [29], [26] or through direct evaluation [23]. In this study, the non-linear force is evaluated at each time step. Two MR-TLCDs are placed in the nacelle, MR-TLCD 1 is placed perpendicular to the rotor plane to mitigate fore-aft vibrations and, MR-TLCD 2 is placed in the nacelle parallel to the rotor plane to mitigate side-to-side vibrations. The equations of motion are again obtained from the total potential and kinetic energy of the coupled system using the Euler-Lagrangian equation. The kinetic energy of the system is given as

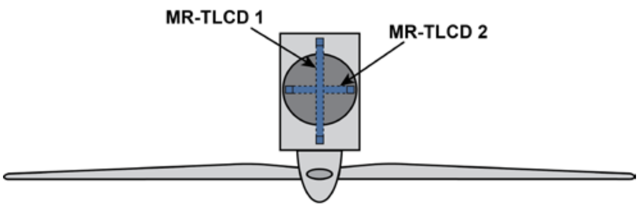

(a) Top view

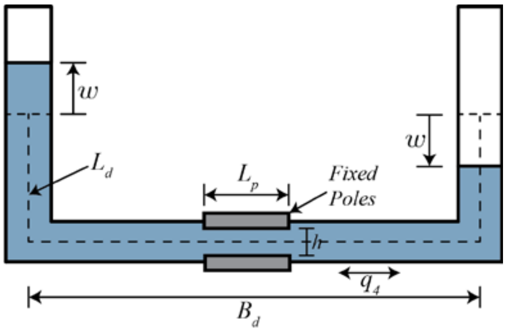

(b) MR-TLCD

Figure 4. HAWT with MR-TLCD

$$T = \frac{1}{2}\sum_{i=1}^{3}\int_0^R \mu(r)|\,\mathbf{v}_{b,i}|^2 dr + \frac{1}{2}\sum_{j=1}^{2}(M_o + m_{d,j})\dot{q}_{4,j}^2 + \frac{1}{2}\sum_{j=1}^{2}\rho_l A_{d,j} L_{d,j}\dot{w}_j^2 \tag{20}$$

The potential energy is given as

$$V = \frac{1}{2}\sum_{i=1}^{3}\sum_{j=1}^{2}\left\{\sum_{k=1}^{2} K_{e,jk} q_{i,j} q_{i,k} + (K_{c,j} + K_{g,j}\cos\psi_i) q_{i,j}^2\right\} + \frac{1}{2}\sum_{j=1}^{2} K_{t,j} q_{4,j}^2 + \sum_{j=1}^{2} g\rho_l A_{d,j} L_{d,j} w_j^2 \tag{21}$$

The generalized set of coordinates are modified according to

$$\tilde{q} = [\, q_{1,1} \quad q_{2,1} \quad q_{3,1} \quad q_{4,1} \quad w_1 \quad q_{1,2} \quad q_{2,2} \quad q_{3,2} \quad q_{4,2} \quad w_2]^T \tag{22}$$

Where, w_j is the liquid displacement of the j^{th} MR-TLCD. The kinetic and potential energy can be substituted in the Euler-Lagrangian equation (7) to obtain the equations of motion. The equations can be written in compact matrix format as

$$\widetilde{M}(t)\ddot{q} + \tilde{C}(t)\dot{q} + \widetilde{K}(t)q = \tilde{f} \tag{23}$$

The generalized forces are also modified with the damping force and the inertial force of the MR-TLCDs as follows

$$\tilde{f}_{4,j} = f_{4,j}^a + f_{4,j}^g - \lambda_j m_{d,j}\ddot{w}_j \tag{24}$$

$$\tilde{f}_{w_j} = -\lambda_j m_{d,j}\ddot{q}_{4,j} - f_{d,j} \tag{25}$$

Where, $m_{d,j}$, λ_j and $f_{d,j}$ is the mass, horizontal length to total length and damping force of the j^{th} MR-TLCD respectively. The non-linear damping force of the MR-TLCD is given as [29]

$$f_{d,j} = -\frac{1}{2}\rho_l A_{d,j}\delta_j\left|\dot{w}_j\right|\dot{w}_j - \frac{c_j\tau_{w,j}A_{d,j}L_{p,j}\dot{w}_j}{h_j\dot{w}_j} = -(u_{p,j} + u_{s,j}) \tag{26}$$

Where, $A_{d,j}$, δ_j, $\tau_{w,j}$, $L_{p,j}$ and h_j are the cross sectional area, head loss coefficient, yield stress of the MR fluid, length of fixed pole and height of liquid between the poles respectively of the j^{th} damper. The damping force of the MR-TLCD is related to the liquid velocity, thus, similar to any passive damper it must be tuned to the natural frequency of the tower for the liquid to be excited under turbulent aerodynamic loads. The tuning ratio or the natural frequency of the tower dictates the liquid length required for the MR-TLCD. The relation between the tuning ratio and liquid length $L_{d,j}$ is given as

$$\omega_{r,j} = \frac{\omega_{d,j}}{\omega_{o,j}} = \sqrt{\frac{2g}{\omega_{o,j}^2 L_{d,j}}} \tag{27}$$

Where, $\omega_{r,j}$, $\omega_{d,j}$ and $\omega_{o,j}$ is the tuning ratio, damper natural frequency, modal frequency of the tower in the j^{th} direction. The equations of motion are written in first order state space form as follows where we separate the damping force from the generalized forces and used them as control inputs.

$$\begin{aligned} \dot{x} &= A(t)x + B(t)u + G(t)\tilde{f} \\ y &= C(t)x \end{aligned} \tag{28}$$

Where, x is the state and the control input vector is given as $u = [f_{d,1} \quad f_{d,2}]^T$. The state matrix and the state vector is given as

$$A(t) = \begin{bmatrix} 0 & I \\ -\widetilde{M}(t)^{-1}\widetilde{K}(t) & -\widetilde{M}(t)^{-1}\tilde{C}(t) \end{bmatrix} \qquad x = [\tilde{q} \quad \dot{\tilde{q}}]^T \tag{29}$$

Where, $\widetilde{M}$, $\tilde{C}$ and $\widetilde{K}$ are the modified mass, damping and stiffness matrices. The matrices are provided in the appendix.

4. Clipped Optimal Control

The infinite time Linear Quadratic Regulator technique has been used here for clipped optimal control. It is clear from equation (28) that the system is time variant. This make the use of classical optimal control methods rather difficult, which is directly applicable only for linear time-invariant systems. To circumvent this problem, in this paper, multiblade coordinate transformation technique has been used to transform the periodic system from its rotating to an equivalent non-rotating framework. This transformation essentially makes the system time-invariant when the time dependent quantities are periodic in nature [20], [28]. This approach has been used here to transform the system in a non-rotating framework where it becomes a LTI system. Thus allowing the use of the classical LQR technique for optimal control. Next, the multiblade coordinate transformation technique is discussed in brief. Reader may refer to [20] for the details.

4.1 Multiblade Coordinate Transformation

The coordinate transformations under this framework of the generalized displacements, velocities and acceleration as given as follows

$$\tilde{q} = \Psi_1 \tilde{q}_{nr} \quad (30)$$

$$\dot{\tilde{q}} = \Psi_1 \dot{\tilde{q}}_{nr} + \Omega\Psi_2 \tilde{q}_{nr} \quad (31)$$

$$\ddot{\tilde{q}} = \Psi_1 \ddot{\tilde{q}}_{nr} + 2\Omega\Psi_2 \dot{\tilde{q}}_{nr} + (\Omega^2\Psi_3 + \dot{\Omega}\Psi_2)\tilde{q}_{nr} \quad (32)$$

Where, Ψ_i's are the transformation matrices provided in the appendix. The subscript nr is used to denote non-rotating framework. The transformation of the state-space matrices are given as follows

$$A_{nr} = \begin{bmatrix} \Psi_1^{-1} & 0 \\ 0 & \Psi_1^{-1} \end{bmatrix} \left\{ A \begin{bmatrix} \Psi_1 & 0 \\ \Omega\Psi_2 & 0 \end{bmatrix} - \begin{bmatrix} \Omega\Psi_2 & 0 \\ \Omega^2\Psi_3 + \dot{\Omega}\Psi_2 & 2\Omega\Psi_2 \end{bmatrix} \right\} \quad (33)$$

$$B_{nr} = \begin{bmatrix} \Psi_1^{-1} & 0 \\ 0 & \Psi_1^{-1} \end{bmatrix} B\Psi_u \quad (34)$$

$$G_{nr} = \begin{bmatrix} \Psi_1^{-1} & 0 \\ 0 & \Psi_1^{-1} \end{bmatrix} G \quad (35)$$

Previous research has shown that sometimes even after the transformation some of the elements remain time dependent. But, averaging the transformed matrices over the rotational time period $\left(T_{rot} = {}^{2\pi}/_{\Omega}\right)$ makes it time invariant without the loss of system properties. The state also needs to be transformed from the rotating to the non-rotating framework. The transformation is given as

$$x = \begin{bmatrix} \Psi_1 & 0 \\ \Omega\Psi_2 & \Psi_1 \end{bmatrix} x_{nr} = T x_{nr} \quad (36)$$

4.2 State feedback controller

Once time averaged in the non-rotating framework a LTI system is obtained in the non-rotating framework that can be written as

$$\dot{x}_{nr} = A_{nr}^{avg} x_{nr} + B_{nr}^{avg} u_{nr} + G_{nr}^{avg} f \quad (37)$$

$$y_{nr} = C_{nr}^{avg} x_{nr} \quad (38)$$

Where, the state x_{nr} and the control input u_{nr} is in non-rotating framework. The cost function must then be written in the non-rotating framework as follows [36]

$$J_c^{nr} = \int_0^\infty (x_{nr}^T Q_{nr} x_{nr} + u_{nr}^T R_{nr} u_{nr}) dt \quad (39)$$

Thus, the control input in non-rotating framework is obtained as

$$u_{nr}^c(t) = -R_{nr}^{-1} B_{nr}^{avg^T} P_{nr} x_{nr}(t) = -K_{nr} x_{nr}(t) \quad (40)$$

Where, K_{nr} is the controller gain called the LQR gain in the non-rotating framework. This is obtained from the solution of the Algebraic Riccati Equation (ARE) given as [36]

$$P_{nr}A_{nr}^{avg} + A_{nr}^{avg^T}P_{nr} - P_{nr}B_{nr}^{avg}R_{nr}^{-1}B_{nr}^{avg^T}P_{nr} + Q_{nr} = 0 \tag{41}$$

The commanded control input thus obtained is in the non-rotating framework. This must be transformed back to the rotating framework given as u_j^c using a transformation matrix. However, since the MR-TLCDs are already in a non-rotating framework, the transformation matrix becomes a 2nd order identity matrix i.e. the commanded control input remains same. It is interesting to note here that, that although the LQR controller is designed here in a non-rotating framework, the transformation before and after the controller essentially results in a periodic controller input. Once the commanded control input is estimated the yield stress of the MR fluid can be estimated from equation (26) as follows

$$\tau_{w,j} = \frac{\left(u_j^c - \frac{1}{2}\rho_l A_{d,j}\delta_j|\dot{w}_j|\dot{w}_j\right)h_j}{c_j A_{d,j} L_{p,j} sgn(\dot{w}_j)} = \frac{\left(u_j^c - u_{p,j}\right)h_j}{c_j A_{d,j} L_{p,j} sgn(\dot{w}_j)} \tag{42}$$

It can be observed from equation (42) that the yield stress can take positive or negative values depending on the signs of u_j^c and $\dot{w}_j$. However, in reality yield stress of the liquid can only take positive values and has a upper limit. For this purpose, an indicator given as $\vartheta_j = u_j^c\dot{w}_j$ is used. Then the yield stress is set to the required value when the indicator is positive or else set to zero when the indicator takes negative values and the desired control input is physically not possible to apply. Thus, the value of the yield stress needs to be estimated at every time step and *clipped* according to the estimation. This application is further simplified by applying the maximum value of yield stress when the indicator is positive rather than setting it to the exact estimated value. Mathematically, it can be given as

$$u_{s,j}(t_i)|_{\vartheta_j>0} = u_{s,j}^{max}\delta[t - t_i] \tag{43}$$

In this above equation, $\delta[\cdot]$ represents the Dirac delta operator. This type of semi-active control where the controller input is restricted by the physical parameters of the device has be terms as *clipped optimal control* in literature, and, the clipping law used here is termed as the *on-off* clipping law.

The infinite time LQR is optimal only when the commanded control input is applied to the system. Here, since the control input is restricted by the physical limitation of the MR-TLCDs it leads to a clipped optimal control strategy. Such heuristic approaches has been successfully used by researches [26], [32] in mitigation of wind induced vibration in multistoried buildings.

5. Fragility Analysis

Fragility analysis is a popular way to assess seismic risk of a structural system. The curves developed for this study denote the conditional probability of a structural demand to reach or exceed a structural capacity under a given level of excitation intensity. Such curves are often used to estimate seismic vulnerability of buildings. This method was used by Dueñas-Osorio and Basu [6] to study the unavailability of wind turbine due to tower accelerations above a threshold value. Quilligan *et al.* [33] has also used fragility analysis to assess the performance of steel and concrete towers. In this study, a power law functional form is used which facilitate the development of fragility curves. The power law model is used to fit simulated peak medians of tower displacements. The power model is given as [6]

$$\hat{d}_v = b(V)^c \tag{44}$$

Where, $\hat{d}_w$ is the median of displacement peaks, V is the wind speed and b and c are constants obtained from linear regression of the data on a logarithmic space. The power model is used to develop fragility curves by providing an estimate of the likelihood of exceeding displacement thresholds as a function of the wind speed. The (conditional) probability of exceeding a predefined displacement limit is described as a lognormal distribution

$$Fragility = P\left[\hat{d}_v \geq d_l | V\right] = 1 - \Phi\left(\frac{ln(d_l) - ln(b(V)^c)}{\beta_{d_v|V}}\right) \tag{45}$$

Where, d_v is the wind-induced in-plane displacement of the blade, d_l are the displacement thresholds and $\beta_{d_v|V}$ is the dispersion of the displacement response as a function of wind speed. For simplicity, the parameter $\beta_{d_v|V}$ is assumed equal to the standard deviation of the displacement response, i.e. it is independent of V.

6. Numerical Results

For numerical simulations, the NREL 5MW baseline offshore wind turbine is used [18]. The wind turbine tower is 87.6m high with three 61.5m long blades. The hub has a radius of 1.5m, which results in a rotor diameter of 120m. The blades made of 8 different airfoils starting with a cylinder at the root and the NACA64 airfoil at its tip. The specifications of the wind turbine is provided in *Table 1*. Sampling rate of 20 Hz is used for the numerical simulations. The 3D wind fields are generated from the TurbSim [17] package distributed by NREL. The wind fields generated account for wind shear and turbulence in the incoming wind. The turbulence intensity level has been kept at 15%. Different mean wind speeds are selected which are uniformly distributed over the operating range of the wind turbine. A schematic diagram of the controller is shown in *Figure 5*.

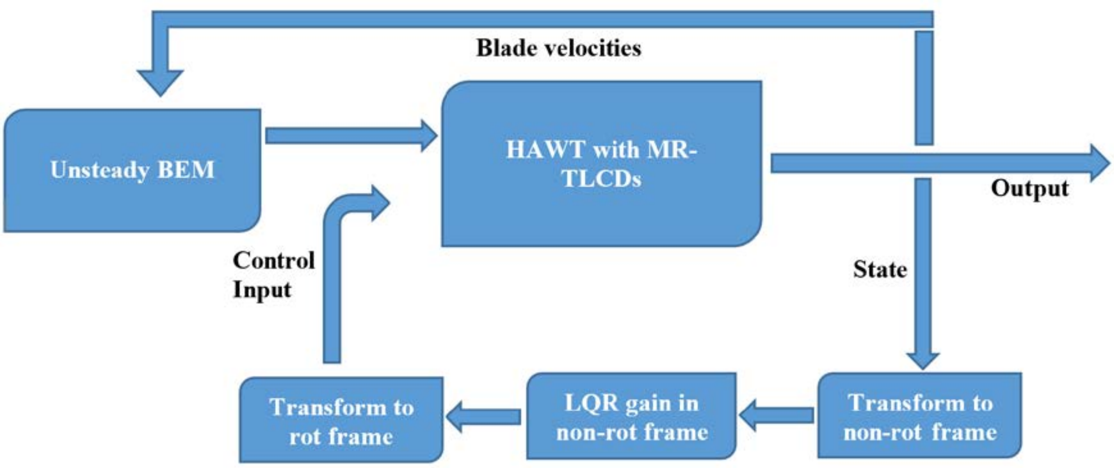

Figure 5. Schematic diagram

Table 1. *Properties of NREL 5-MW baseline HAWT*

NREL 5-MW baseline wind turbine properties		
Basic description	Max. rated power	5-MW
	Rotor orientation, configuration	Upwind, 3 blades
	Rotor diameter	126m
	Hub height	90m
	Cut-in, rated, cut-out wind speed	3m/s, 11.4m/s, 25m/s
	Cut-in, rated rotor speed	6.9rpm, 12.1 rpm
Blade (LM 61.5 P2)	Length	61.5m
	Overall (integrated) mass	17 740 kg
	Second mass moment of inertia	11 776 kg m^2
	1st in-plane mode natural frequency	1.0606 Hz
	1st out-of-plane mode natural frequency	0.6767 Hz
	Structural-damping ratio(all modes)	0.48%
Hub + Nacelle	Hub diameter	3m
	Hub mass	56 780 kg
	Nacelle mass	240 000 kg
Tower	Height above ground	87.6m
	Overall (integrated) mass	347 460 kg
	1st Fore-Aft mode natural frequency	0.324 Hz
	1st Side-to-Side mode natural frequency	0.312 Hz
	Structural-damping ratio(all modes)	1%

Two MR-TLCDs are placed in the nacelle; MR-TLCD 1 is placed perpendicular to rotor plane to mitigate fore-aft tower vibrations and, MR-TLCD 2 parallel to rotor plane to mitigate side-to-side tower vibrations. The proposed arrangement is shown in Figure 4(a). Both the MR-TLCDs have a mass of 1% of the nacelle-hub assembly. The liquid length required for both the MR-TCLDs is 5.04m, which results from equation (27) by substituting the tower frequency of 0.314Hz. The depth of the nacelle is ~14.5m, which allows enough length to place MR-TLCD 1. The horizontal to total length ratio (λ_1) of MR-TLCD 1 is chosen as 0.85. This leads to a horizontal length ($B_{d,1}$) of 4.3m. The width of the nacelle is ~4.2m, due to the shorter dimension in this direction, the horizontal to total length ratio (λ_2) of MR-TLCD 2 is chosen as 0.75. This leads to a horizontal length ($B_{d,2}$) of 3.8m.

Table 2. *MR-TLCD properties*

Properties	**MR-TLCD 1**	**MR-TLCD 2**
Fluid density (ρ_l in kg/m^3)	2500	2500
Constant depending on flow velocity (c)	2.1	2.1
Length of fixed poles (L_p in m)	0.5	0.5
Horizontal to total length ratio (λ)	0.85	0.75
Distance between poles (h in m)	0.3	0.3
Length of liquid column (L_d in m)	5.04	5.04
Horizontal length of liquid column (B_d in m)	4.3	3.8
Cross-sectional area (A_d in m^2)	0.235	0.235
Head loss coefficient (δ)	1	1
Yield stress of the liquid (τ_w in N/m^2)	50	90

It must be noted here that previous research [34] has shown that lower value of λ_j has detrimental effect on the performance of TLCDs, and hence MR-TLCDs. The details of the MR-TLCD parameters are provided in Table 2. Before evaluating the performance of the controllers an attempt is made to validate the fully fixed wind turbine model. The NREL distributed wind turbine analysis package FAST developed by Jonkman and Buhl [39] is used to benchmark the 8 DOF fixed base system developed in the previous section, using the NREL 5 MW reference offshore wind turbine Jonkman BJ et al. [18]. A comparison is made between the predicted modal frequencies from the developed HAWT model and FAST for the 8 DOF wind turbine model. In FAST modal frequencies for the system are obtained by performing an Eigen analysis on the first order state matrix created from a linearization analysis. Using a similar method (generating the system matrix A from the derived model), the modal frequencies for the developed modal are calculated. *Table 3* lists the modal frequencies for each DOF. Examining *Table 3*, we see that the results agree well.

Table 3. *Comparison of developed model to FAST.*

Model	**Blade Frequencies (Hz)**		**Tower Frequencies (Hz)**	
	In-plane	Out-of-plane	In-plane	Out-of-plane
FAST	1.123	0.738	0.326	0.315
Derived Model	1.091	0.733	0.314	0.314

With the MR-TLCDs placed and tuned to the towers natural frequency numerous aeroelastic simulations are carried out to evaluate the performance of the semi-active controllers. It is again important to note here that the MR-TLCD parameters are the same for the entire operational range of the wind turbine. *Figure 6* shows the tower fore-aft response time history under turbulent wind at the rated wind speed with and without the MR-TLCD. It can be observed that the response is highly damped and not much reduction is achieved here. The Fourier amplitude of the tower fore-aft response is shown in *Figure 7*. It can be observed here that the MR-TLCD 1 has effectively damped the amplitudes associated to the tower natural frequency. Since, the response is highly damped; the energy associated with its natural frequency is relatively less, which results in a 8.5% reduction of the RMS value of the response. Increasing the mass ratio to 2% or even 5% will further reduce the response amplitudes but the gain obtained is not worth the cost. Thus, it can be concluded that for the highly damper fore-aft response, an external damper does not improve the response significantly.

Figure 8 and *Figure 9* shows the tower side-to-side response time history and the Fourier amplitude spectrum respectively with and without the MR-TLCD. Unlike the fore-aft response, the side-to-side response is very lightly damped. Thus, the external damper offers considerable improvement in the response with a reduction of 46.2% in its RMS value. It can be observed that much of the energy in the response is associated with the natural frequency of the tower and, in small bits distributed over the loading frequencies and the blade-tower coupled frequencies. In this case and MR-TLCD with 1% mass ratio attains high levels of response reductions.

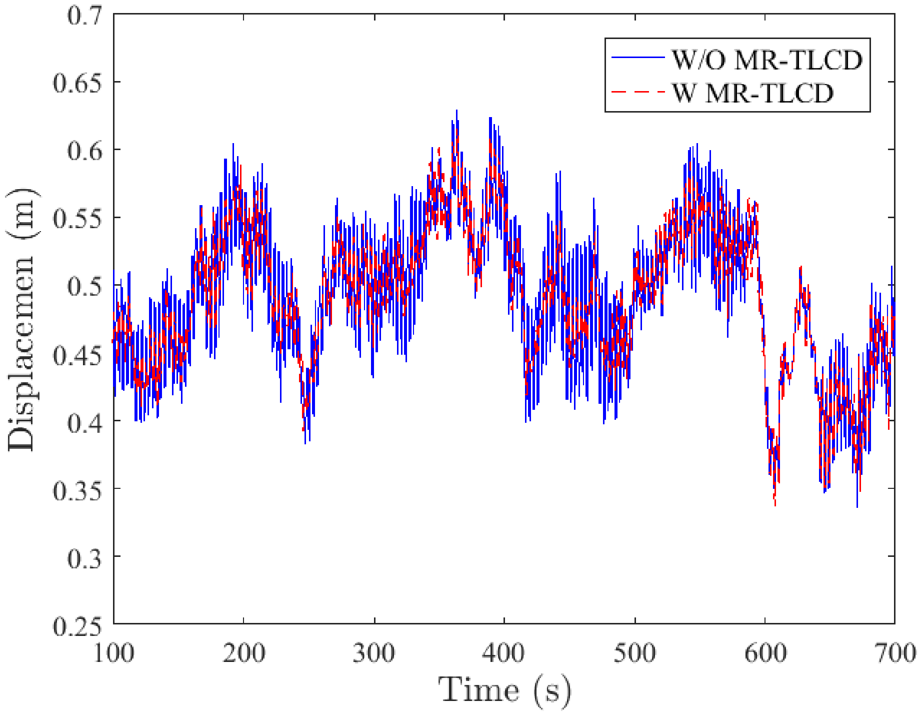

Figure 6. Tower fore-aft response time history

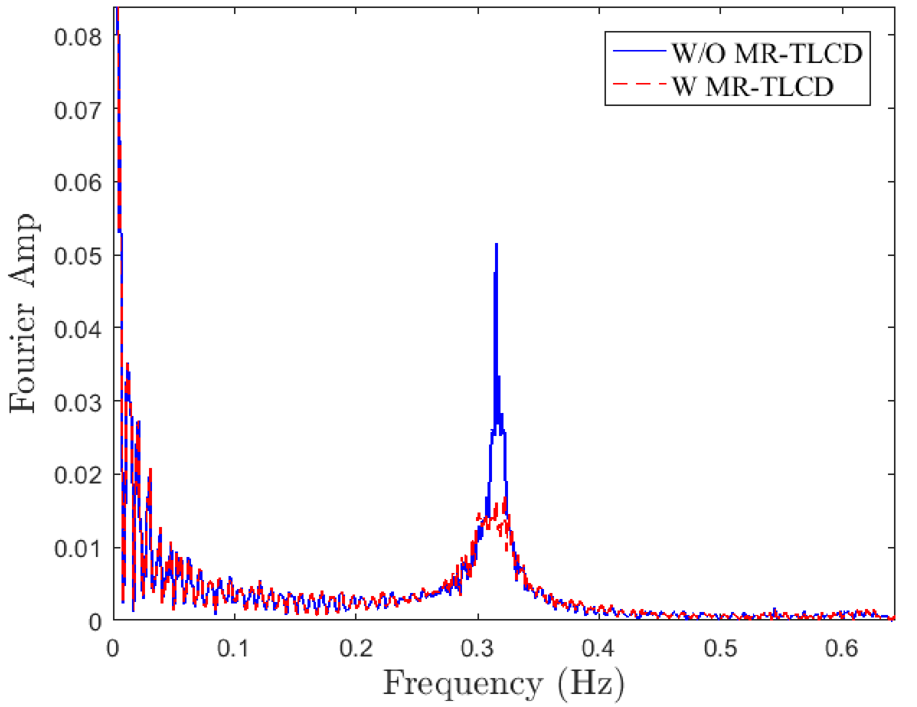

Figure 7. Tower fore-aft response Fourier amplitude spectrum

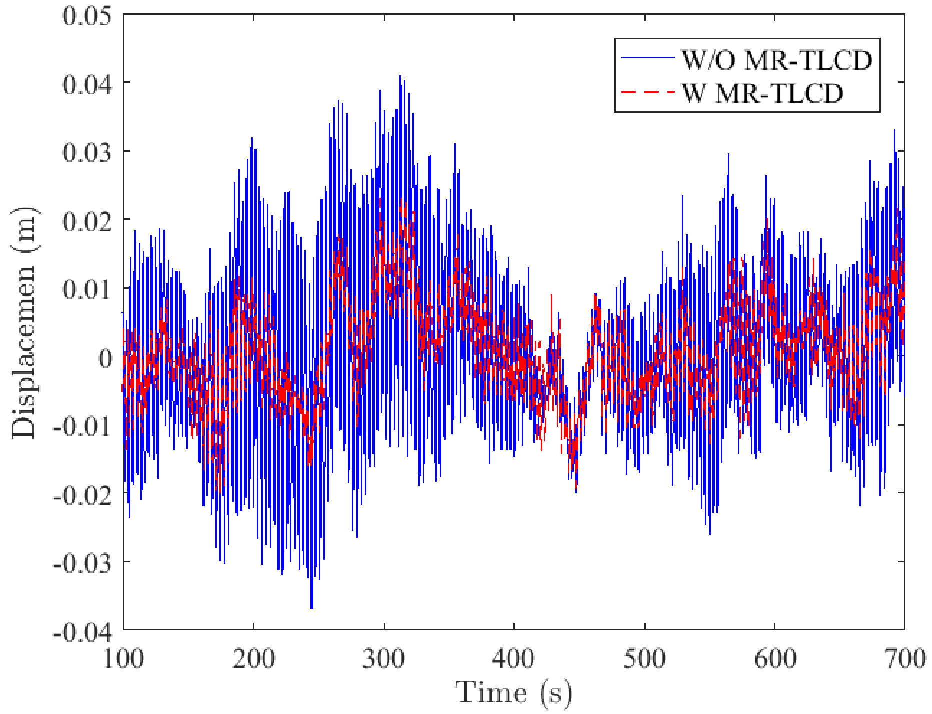

Figure 8. Tower side-to-side response time history

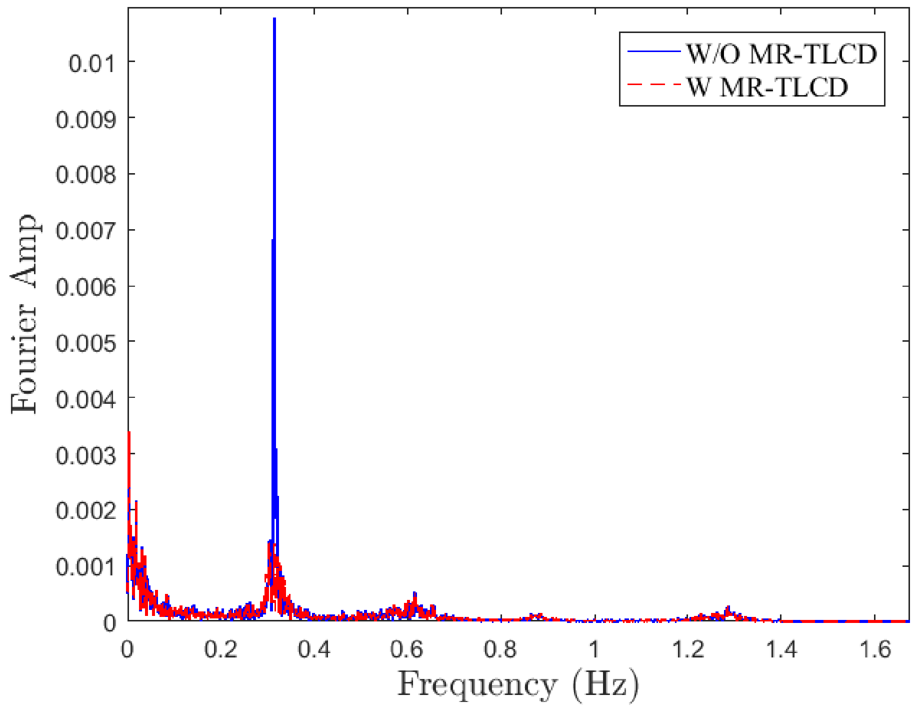

Figure 9. Tower side-to-side response Fourier amplitude spectrum

Consistent with the discussion held above, the reductions in the peak medians of the tower fore-aft and side-to-side responses with and without the MR-TLCDs are shown in *Figure 10* and *Figure 11* respectively. The circles in both the figures denote the simulated results and the solid lines denote the peaks obtained from linear regression in a logarithmic space. These figures show the reductions achieved in the entire operational range.

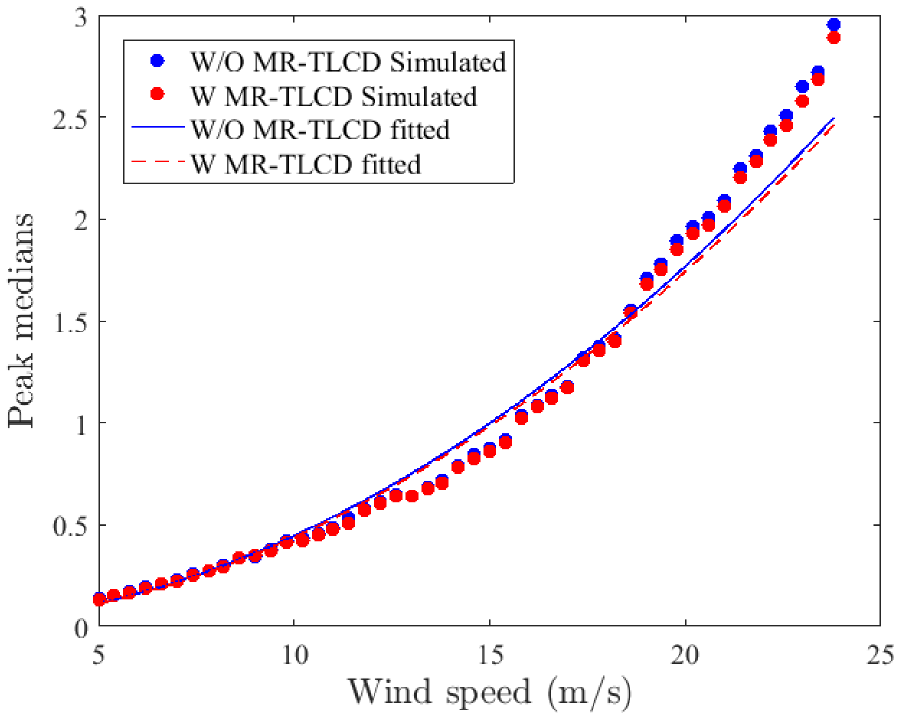

Figure 10. Medians of tower fore-aft peak displacements

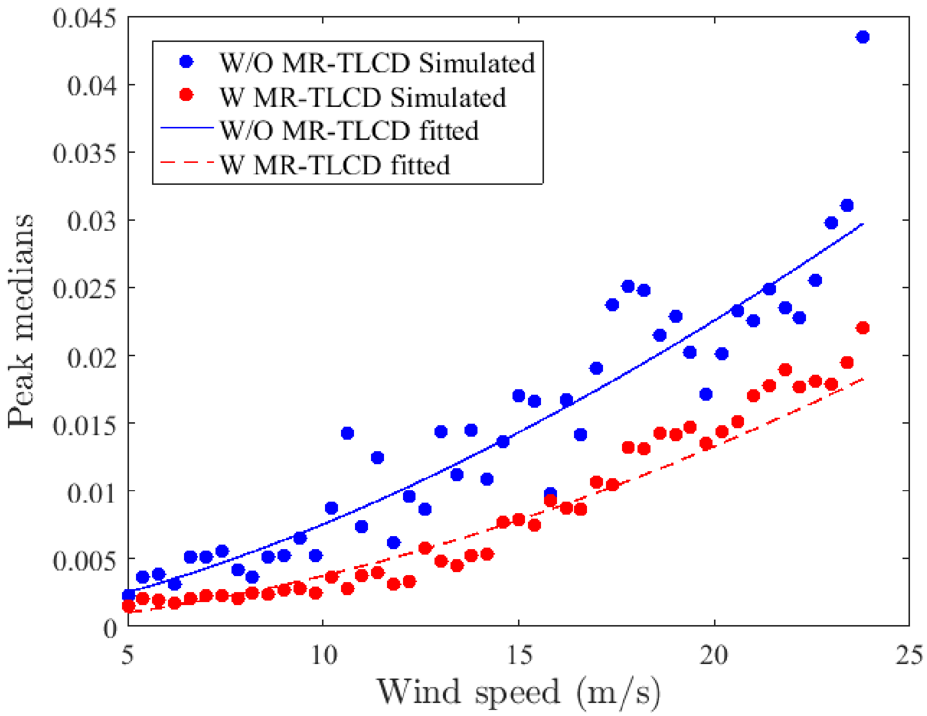

Figure 11. Medians of tower side-to-side peak displacements

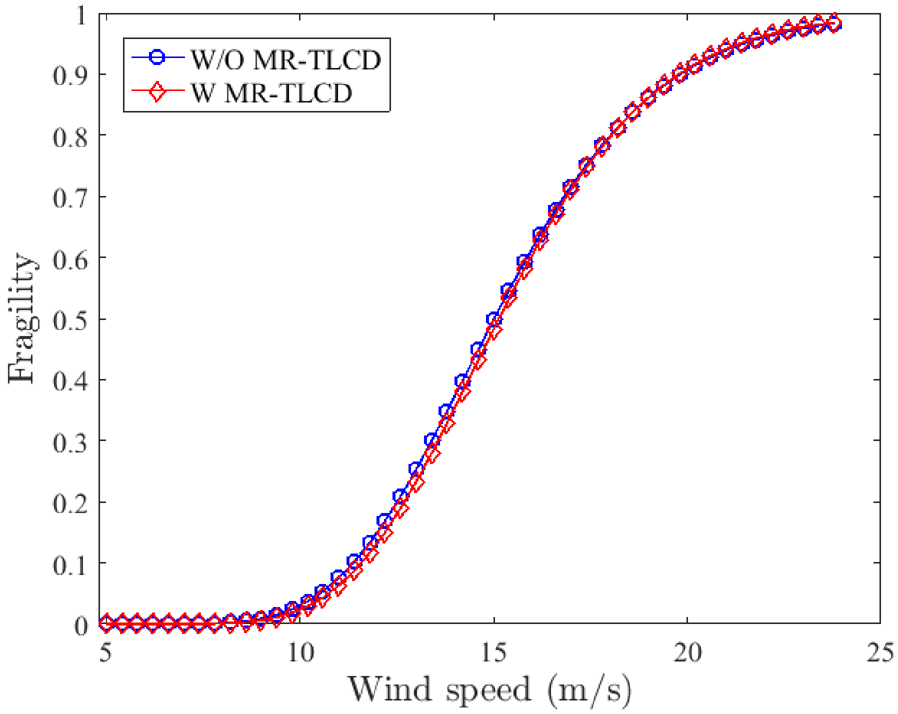

Figure 12. Fragility curve for tower fore-aft response at $d_l = 1.0$m

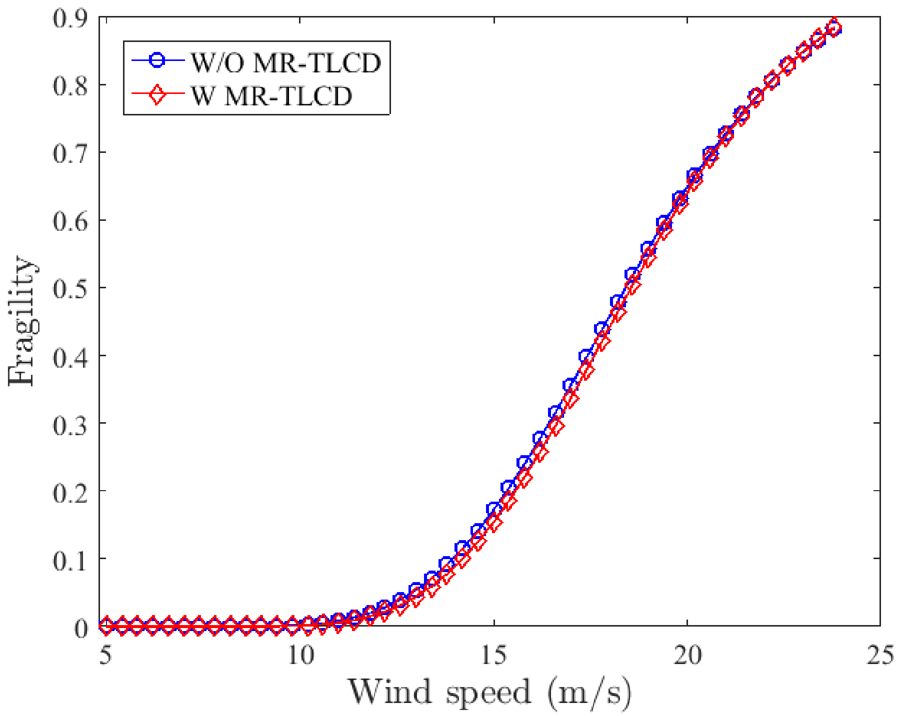

Figure 13. Fragility curve for tower fore-aft response at $d_l = 1.5$m

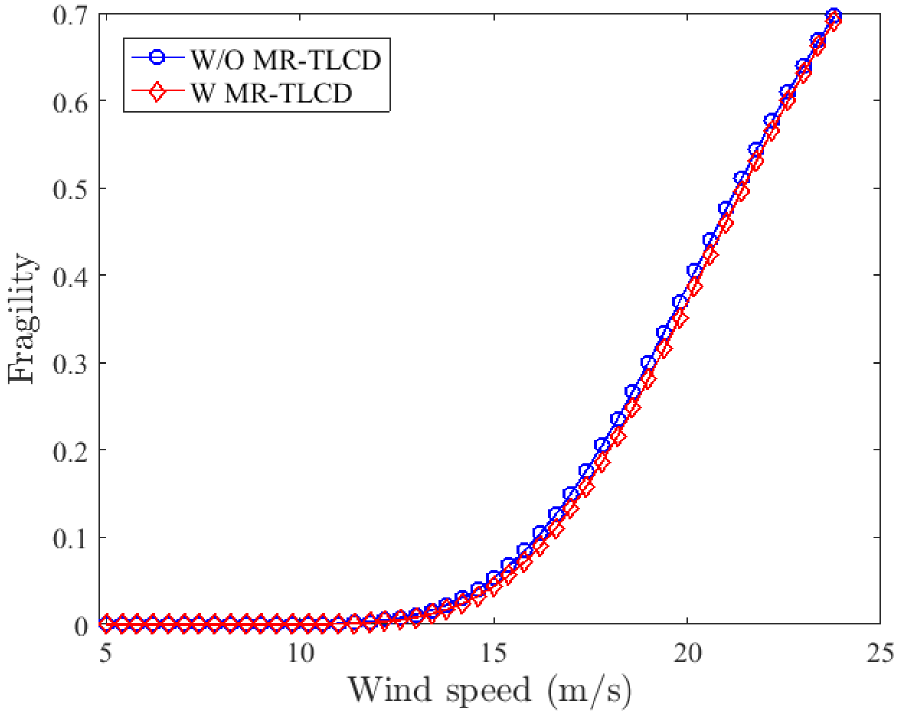

Figure 14. Fragility curve for tower fore-aft response at $d_l = 2.0$m

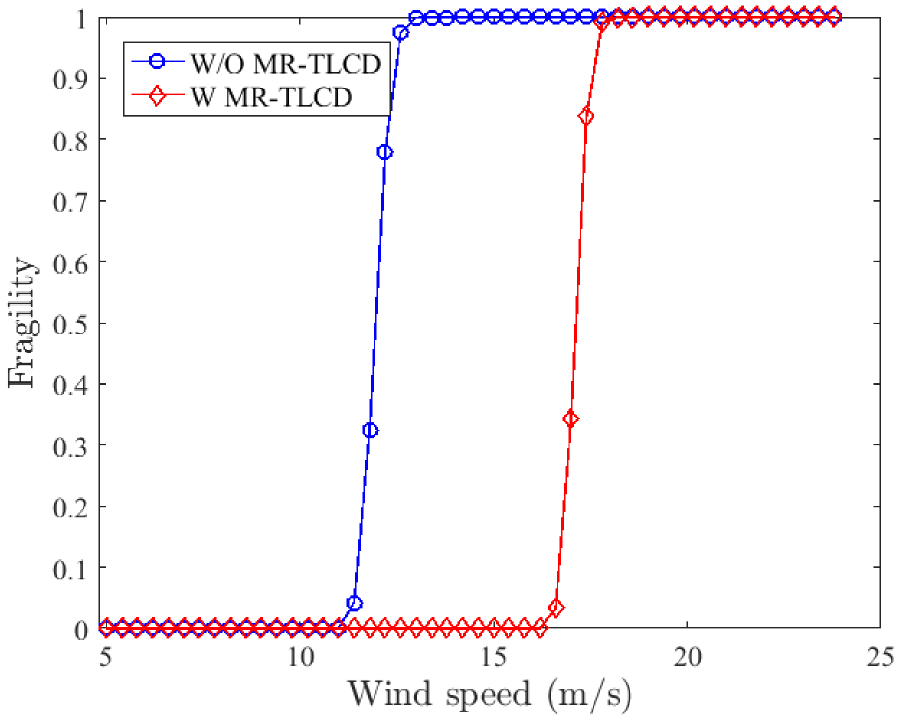

Figure 15. Fragility curve for tower side-to-side response at $d_l = 0.01$m

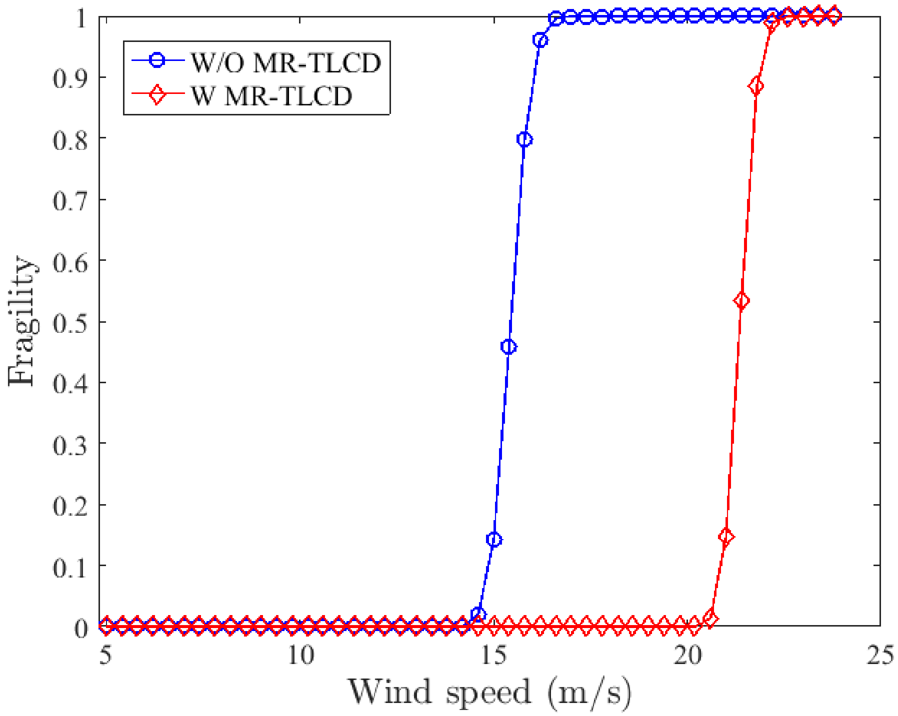

Figure 16. Fragility curve for tower side-to-side response at $d_l = 0.015$m

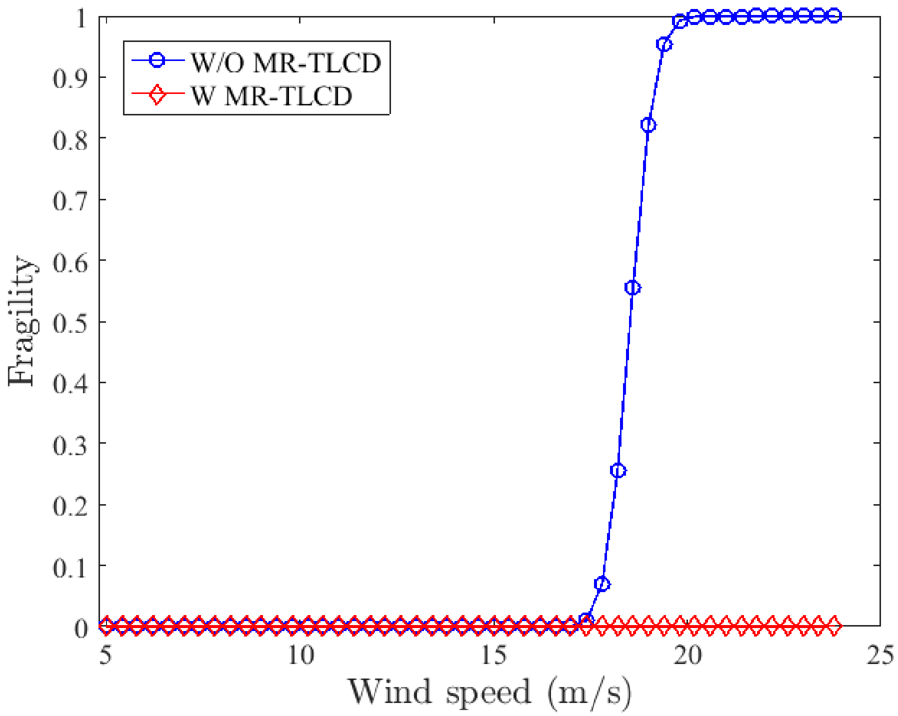

Figure 17. Fragility curve for tower side-to-side response at $d_l = 0.02$m

Similar to the response reductions observed previously, the reductions of peak medians for the fore-aft the response is not significant over the entire operating range of the wind turbine as shown in *Figure 10*. The reductions in fore-aft response decreases at high wind speed due to the increase aerodynamic damping. However, significant reductions are observed in *Figure 11* for tower side-to-side responses. The power law models are excellent fits for the simulated response data with coefficients of determination R^2 with values of 0.988, 0.910, 0.988 and 0.932, respectively for uncontrolled tower fore-aft and side-to-side responses and, controlled tower fore-aft and side-to-side responses. *Figure 12*, *Figure 13* and *Figure 14* gives the fragility curves for tower fore-aft peak displacements for threshold displacements (limit states) of 1.0m, 1.5m and 2.0m respectively. The figures demonstrate small reductions in the probability of exceeding the displacement limit states of the fore-aft motion with MR-TLCD 1 as compared to without the damper. For instance at rated wind speed of 11.4m/s the conditional probability of exceeding the displacement of 1.0m is reduced from 10.2% to 8.7%. Similar results were also presented by [16].

The fragility curves for the tower side-to-side displacement are shown in *Figure 15*, *Figure 16* and *Figure 17* respectively for limit states of 0.01m, 0.015m and 0.02m. It can be observed that the displacement peaks are highly sensitive to wind speed where, the probability of exceeding the threshold displacement sudden increases from almost zero to one within a very small span. The installation of the dampers shifts this exceedance to a much higher wind speed compared to a tower without the MR-TLCD.

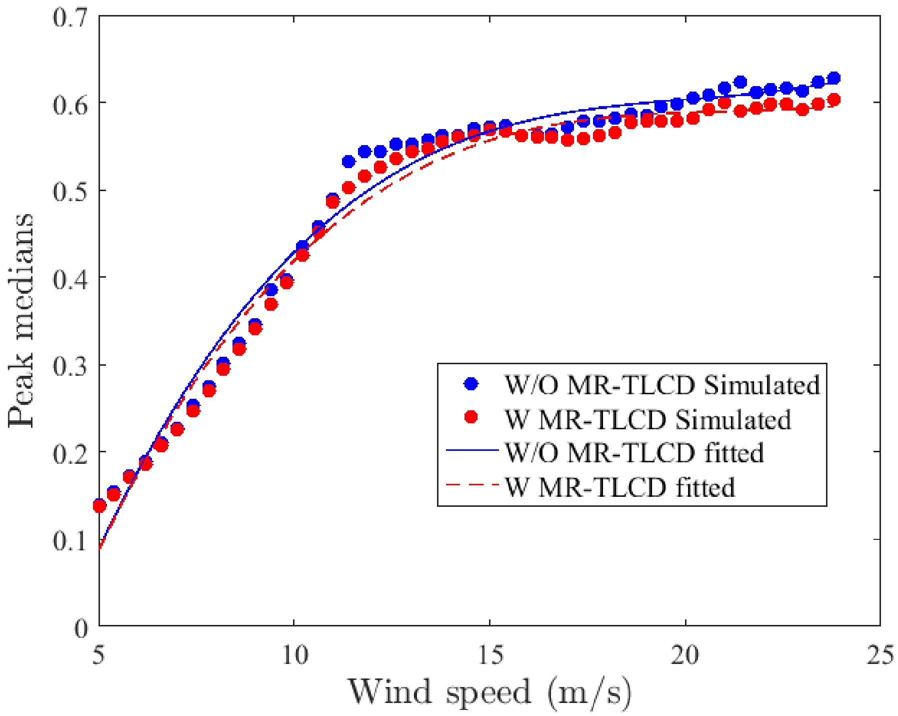

Figure 18. Medians of tower fore-aft peak displacements for pitch controlled WT

The discussion held thus far pertains to a wind turbine which is not pitch controlled and the pitch angle is neglected during its operation. Under practical circumstances a wind turbine will always be pitch controlled to stabilize the power production. Literature available on fragility analysis of wind turbines so far have not considered the pitch angle. In this paper, an attempt is made to address this issue is. Jonkman *et al*.[18] summarises the pitch angles at different wind speed required for stable power production of the 5MW wind turbine. As is understood from the BEM theory, the thrust is decreased by introducing a pitch angle. *Figure 18* shows the peak median of the fore-aft response. It is clear that the pitch angle has decreased the aerodynamic thrust and the fore-aft displacements are reduced. Unlike the pervious case, the fore-aft response does not have a parabolic increase, rather, it approaches a constant value. Also, for a pitch controlled wind turbine the reductions do not drop at increased wind speeds. This is due to the fact the reduced thrust decreases the aerodynamic damping. The peak medians of the side-to-side response still has a parabolic increase as shown in *Figure 19*, but with a slightly higher rate of increase. Very good reductions are achieve by the damper over its operational range. The power law model used previously to fit the simulated results. This was done by linear regression on a logarithmic space. But, the same approach did not produce good fit in this case. So, instead of the power law model, a 3rd order polynomial is fitted to the simulated data which is then used for fragility analysis.

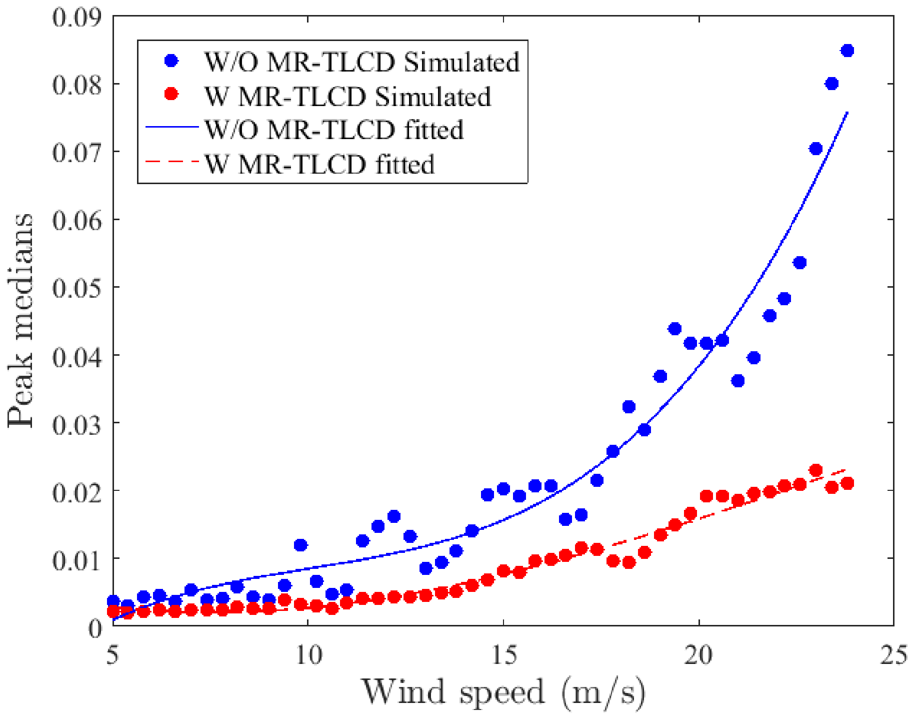

Figure 19. Medians of tower side-to-side peak displacements for pitch controlled WT

The fragility curves for the fore-aft response is shown in *Figure 20*. The limit state is redefined since there is a big difference in magnitudes of displacements between a pitch controlled and uncontrolled wind turbine tower. For a threshold displacement of 0.5m at rated wind speed the probability of exceeding the limit state is decreased from 31% to 19%. Therefore for a pitch controlled wind turbine the MR-TLCD 1 works much better in improving structural reliability. The fragility curves for side-to-side response is shown in *Figure 21*. The curves look similar to the previous results. But here, the probability of exceeding the threshold displacement increases even faster from almost zero to one within a very small span. This is due to increased rate of displacement increment caused by the introduction of pitch angles. The performance of the MR-TLCDs in the whole operational range justifies their use in multi-megawatt wind turbines.

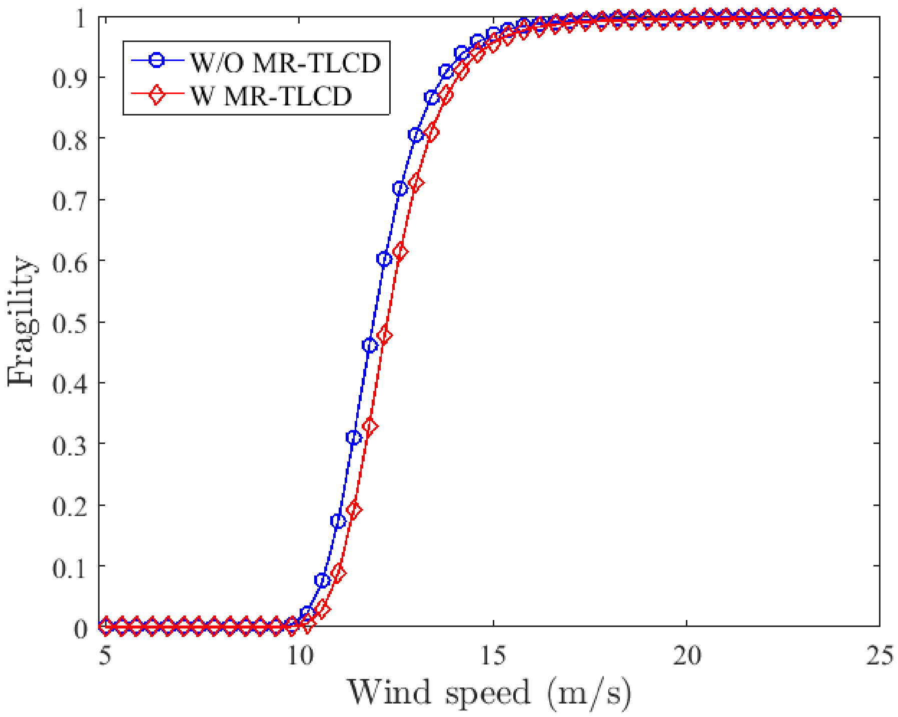

Figure 20. Fragility curve for pitch controlled tower fore-aft response at $d_l = 0.5$m

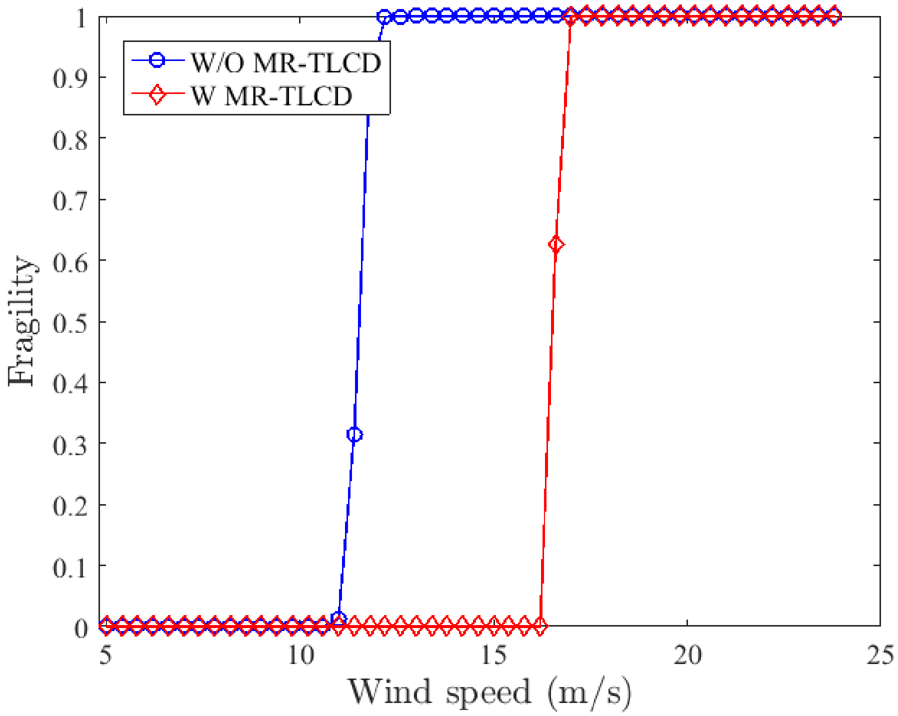

Figure 21. Fragility curve for pitch controlled tower side-to-side response at $d_l = 0.01$m

Conclusions

This paper deals with vibration control of wind turbine tower using MR-TLCDs. The smart damper advantages of the MR-TLCD over a conventional TLCD are used to reduce tower fore-aft and side-to-side motion under turbulent aerodynamic loads. Fragility analysis is used as a tool to evaluated the improved reliability of the tower when installed with MR-TLCDs. The main contributions of this study are mentioned below.

- The wind turbine experiences considerable aerodynamic damping in its fore-aft mode. Hence, an external damper does not offer high reductions in the response.
- For the side-to-side motion, the MR-TLCD efficiently arrests the excessive vibrations since it is very lightly damped.
- Fragility analysis show that the dampers offer small improvement in reliability of the tower fore-aft motion and remarkable improvement in reliability of the tower side-to-side motion.
- In this paper, the fragility curves of a pitch controlled wind turbine is also studied.
- For a pitch controlled wind turbine, there is considerable decrease in thrust above rated wind speed. Hence, the aerodynamic damping reduces and the MR-TLCD 1 works better to mitigate the fore-aft vibrations. MR-TLCD 2 still works excellently to control the side-to-side vibrations.
- For a pitch controlled wind turbine, MR-TLCD 1 offer more improvement in reliability of the tower fore-aft motion than in wind turbine without pitch control.

References

[1] **Council GWE.** *Global wind energy outlook 2016*. GWEC, November 2016.

[2] **GWEC.** *Global Wind Energy Report: Annual Market Update 2015.* Global Wind Energy Council; 2015.

[3] **GWEC.** *Global Wind Report 2006.* Global Wind Energy Council; 2006.

[4] **Ahlstrøm A.** *Influence of wind turbine flexibility on loads and power production.* Wind Energy; **9**(3):237-49. 2006.

[5] **Colwell S, Basu B.** *Tuned liquid column dampers in offshore wind turbines for structural control.* Engineering Structures; **31**(2):358-68. 2009.

[6] **Dueñas-Osorio L, Basu B**. *Unavailability of wind turbines due to wind induced accelerations.* Engineering Structures; **30**(4):885-93. 2008.

[7] **Chou JS, Tu WT.** *Failure analysis and risk management of a collapsed large wind turbine tower.* Engineering Failure Analysis. **18**(1):295- 313. 2011.

[8] **Murtagh PJ, Ghosh A, Basu B, Broderick BM**. *Passive control of wind turbine vibrations including blade/tower interaction and rotationally sampled turbulence.* Wind Energy; **11**(4): 305-17. 2008.

[9] **Lackner MA, Rotea MA.** *Passive structural control of offshore wind turbines.* Wind Energy; **14**(3):373-88. 2011.

[10] **Lackner MA, Rotea MA**. *Structural control of floating wind turbines.* Mechatronics; **21**(4):704-19. 2011

[11] **Arrigan J, Pakrashi V, Basu B, Nagarajaiah S.** *Control of flapwise vibrations in wind turbine blades using semi-active tuned mass dampers.* Structural Control and Health Monitoring; **18**(8):840-51. 2011.

[12] **Fitzgerald B, Basu B.** *Structural control of wind turbines with soil structure interaction included.* Engineering Structures; **111**: 131-51. 2016.

[13] **Fitzgerald B, Basu B, Nielsen SRK.** *Active tuned mass dampers for control of in-plane vibrations of wind turbine blades.* Structural Control and Health Monitoring; 2013.

[14] **Fitzgerald B, Basu B.** *Cable connected active tuned mass dampers for control of in-plane vibrations of wind turbine blades.* Journal of Sound and Vibration; **333**(23):5980-6004. 2014.

[15] **Staino A, Basu B, Nielsen S.** *Actuator control of edgewise vibrations in wind turbine blades.* Journal of Sound and Vibration. **331**(6):1233-56. 2012.
[16] **Mensah AF, Dueñas-Osorio L.** *Improved reliability of wind turbine towers with tuned liquid column dampers (TLCDs).* Structural Safety; **47**:78-86. 2014.
[17] **Kelley ND, Jonkman BJ.** *Overview of the TurbSim stochastic inflow turbulence simulator.* National Renewable Energy Laboratory; 2005.
[18] **Jonkman JM, Butterfield S, Musial W, Scott G.** *Definition of a 5-MW Reference Wind Turbine for Offshore System Development.* National Renewable Energy Laboratory, Technical Report, NREL/TP-500-38060, Golden, Colorado; 2009.
[19] **Hansen MO.** *Aerodynamics of wind turbines.* Routledge; 2015.
[20] **Bir G**; *Multiblade coordinate transformation and its application to wind turbine analysis*. In: ASME Wind Energy Symposium. 2008.
[21] **Burton T, Sharpe D, Jenkins N and Bossanyi E**; Wind energy handbook. John Wiley & Sons. 2001.
[22] **Colwell S and Basu B**; *Tuned liquid column dampers in offshore wind turbines for structural control.* Engineering Structures. 2009.
[23] **Di Matteo A, Iacono FL, Navarra G and Pirrotta A**; *Direct evaluation of the equivalent linear damping for TLCD systems in random vibration for pre-design purposes.* International Journal of Non-Linear Mechanics **63**: 19–30. 2014.
[24] **Lewis FL and Syrmos VL**; *Optimal control*. John Wiley & Sons. 1995.
[25] **Moriarty PJ and Hansen AC**. *AeroDyn theory manual.* National Renewable Energy Laboratory Golden, Colorado, USA. 2005.
[26] **Ni Y, Ying Z, Wang J, Ko J and Spencer B**; *Stochastic optimal control of wind-excited tall buildings using semi-active MRTLCDs.* Probabilistic Engineering Mechanics **19**(3): 269–277. 2004.
[27] **Sakai F, Takaeda S and Tamaki T**; *Tuned liquid column damper-new type device for suppression of building vibrations.* In: International Conference on Highrise Buildings, Nanjing, China, Mar. pp. 25–27. 1989.
[28] **Stol KA, Moll HG, Bir G and Namik H;** *A comparison of multi-blade coordinate transformation and direct periodic techniques for wind turbine control design*. In: Proceedings of the 47th AIAA/ASME. 2009.
[29] **Wang J, Ni Y, Ko J and Spencer B**; *Magneto-rheological tuned liquid column dampers (MR-TLCDs) for vibration mitigation of tall buildings: modelling and analysis of open-loop control.* Computers & structures **83**(25): 2023–2034. 2005.
[30] **Wu JC, Shih MH, Lin YY and Shen YC;** *Design guidelines for tuned liquid column damper for structures responding to wind.* Engineering Structures **27**(13): 1893–1905. 2005.
[31] **Yalla SK and Kareem A**; *Optimum absorber parameters for tuned liquid column dampers.* Journal of Structural Engineering. **126**(8): 906–915. 2000.
[32] **Yalla SK, Kareem A and Kantor JC**; *Semi-active tuned liquid column dampers for vibration control of structures.* Engineering Structures **23**(11): 1469–1479. 2001.
[33] **Quilligan A, O'Connor A, Pakrashi V**. *Fragility analysis of steel and concrete wind turbine towers.* Eng Structures; **36**:270–82. 2012.
[34] **Balendra T,Wang C and Cheong H.** *Effectiveness of tuned liquid column dampers for vibration control of towers.* Engineering Structures **17**(9): 668–675. 1995.
[35] **Burton T, Sharpe D, Jenkins N and Bossanyi E**. *Wind energy handbook.* John Wiley & Sons. 2001.
[36] **Lewis FL and Syrmos VL**. *Optimal control.* John Wiley & Sons. 1995.
[37] **Buhl, M. L**., *A New Empirical Relationship between Thrust Coefficient and Induction Factor for the Turbulent Windmill State*, Tech. Rep. NREL/TP-500-36834, National Renewable Energy Laboratory, Aug 2005.
[38] **Ning, A**., *A Simple Solution Method for the Blade Element Momentum Equations with Guaranteed Convergence*, Wind Energy, Vol. **17**, No. 9, pp. 1327–1345, Sep 2014.
[39] **Jonkman JM & Buhl ML Jr**., *FAST users guide*. *Report No. NREL/EL-500-38230*, National Renewable Energy Laboratory, Golden, CO, USA, 2005.

Appendix

The mass damping and stiffness matrices of the combined blade-tower is given by

$$M(t)=\begin{bmatrix} m_{2,1} & 0 & 0 & m_{1,1} & 0 & 0 & 0 & 0 \\ 0 & m_{2,1} & 0 & m_{1,1} & 0 & 0 & 0 & 0 \\ 0 & 0 & m_{2,1} & m_{1,1} & 0 & 0 & 0 & 0 \\ m_{1,1} & m_{1,1} & m_{1,1} & m_{3,1} & 0 & 0 & 0 & 0 \\ 0 & 0 & 0 & 0 & m_{2,2} & 0 & 0 & a_1 \\ 0 & 0 & 0 & 0 & 0 & m_{2,2} & 0 & a_2 \\ 0 & 0 & 0 & 0 & 0 & 0 & m_{2,2} & a_3 \\ 0 & 0 & 0 & 0 & a_1 & a_2 & a_3 & m_{3,2} \end{bmatrix}$$

Where $a_i \;= m_{1,2}\,\cos\psi_i$ for i =1, 2, 3

$$C(t)=\begin{bmatrix} c_{b,1} & 0 & 0 & 0 & 0 & 0 & 0 & 0 \\ 0 & c_{b,1} & 0 & 0 & 0 & 0 & 0 & 0 \\ 0 & 0 & c_{b,1} & 0 & 0 & 0 & 0 & 0 \\ 0 & 0 & 0 & c_{t,1} & 0 & 0 & 0 & 0 \\ 0 & 0 & 0 & 0 & c_{b,2} & 0 & 0 & b_1 \\ 0 & 0 & 0 & 0 & 0 & c_{b,2} & 0 & b_2 \\ 0 & 0 & 0 & 0 & 0 & 0 & c_{b,2} & b_3 \\ 0 & 0 & 0 & 0 & b_1 & b_2 & b_3 & c_{t,2} \end{bmatrix}$$

Where $b_i \;=$ -2$\Omega m_{1,2}\,\sin\psi_i$ for i =1, 2, 3

$$K(t)=\begin{bmatrix} k_{1,1} & 0 & 0 & 0 & k_{12} & 0 & 0 & 0 \\ 0 & k_{2,1} & 0 & 0 & 0 & k_{12} & 0 & 0 \\ 0 & 0 & k_{3,1} & 0 & 0 & 0 & k_{12} & 0 \\ 0 & 0 & 0 & k_{t,1} & 0 & 0 & 0 & 0 \\ k_{12} & 0 & 0 & 0 & k_{1,2} & 0 & 0 & c_1 \\ 0 & k_{12} & 0 & 0 & 0 & k_{2,2} & 0 & c_2 \\ 0 & 0 & k_{12} & 0 & 0 & 0 & k_{3,2} & c_3 \\ 0 & 0 & 0 & 0 & c_1 & c_2 & c_3 & k_{t,2} \end{bmatrix}$$

Where, $c_i \;=$ -$\Omega^2 m_{1,2}\,\cos\psi_i$, for $i=1$, 2, 3. The terms in $M(t)$ matrix are $m_{1,1}=\int_0^R \mu(r)\phi_1 dr,\; m_{2,1}=\int_0^R \mu(r)\phi_1^2 dr,\; m_{3,1}=3\int_0^R \mu(r)dr+M_{o,1}+M_n+M_h,\; m_{1,2}\;=\int_0^R \mu(r)\phi_2 dr,\; m_{2,2}=\int_0^R \mu(r)\phi_2^2 dr,$ $m_{3,2}=3\int_0^R \mu(r)dr+M_{o,2}+M_n+M_h$. Here subscripts o,n and h represents the modal mass of the tower and nacelle and hub mass respectively. The stiffness terms are given as, $k_{i,1}=k_{e,1}+k_{c,1}+k_{g,1}\cos\psi_i$ and $k_{i,2}=k_{e,2}+k_{c,2}+k_{g,2}\cos\psi_i-\Omega^2 m_{2,2}$ where subscripts e,g and c represents elastic, gravitational and centrifugal stiffness of the blades respectively and $k_{t,1}$ and $k_{t,2}$ represents the stiffness of the tower in out-of-plane and in-plane directions respectively. The terms $c_{b,1}$, $c_{t,1}$ and $c_{b,2}$, $c_{t,2}$ in the C matrix denote the damping associated with the blades and the nacelle in the out-of-plane and in-plane directions respectively. The combined HAWT tower-MR-TLCD matrices are as follows

$$\widetilde{M}(t)=\begin{bmatrix} m_{2,1} & 0 & 0 & m_{1,1} & 0 & 0 & 0 & 0 & 0 & 0 \\ 0 & m_{2,1} & 0 & m_{1,1} & 0 & 0 & 0 & 0 & 0 & 0 \\ 0 & 0 & m_{2,1} & m_{1,1} & 0 & 0 & 0 & 0 & 0 & 0 \\ m_{1,1} & m_{1,1} & m_{1,1} & m_{3,1}+m_{d1} & \lambda_1 m_{d1} & 0 & 0 & 0 & 0 & 0 \\ 0 & 0 & 0 & \lambda_1 m_{d1} & m_{d1} & 0 & 0 & 0 & 0 & 0 \\ 0 & 0 & 0 & 0 & 0 & m_{2,2} & 0 & 0 & a_1 & 0 \\ 0 & 0 & 0 & 0 & 0 & 0 & m_{2,2} & 0 & a_2 & 0 \\ 0 & 0 & 0 & 0 & 0 & 0 & 0 & m_{2,2} & a_2 & 0 \\ 0 & 0 & 0 & 0 & 0 & a_1 & a_2 & a_3 & m_{3,2}+m_{d2} & \lambda_2 m_{d2} \\ 0 & 0 & 0 & 0 & 0 & 0 & 0 & 0 & \lambda_2 m_{d2} & m_{d2} \end{bmatrix}$$

$$\tilde{C}(t)=\begin{bmatrix} c_{b,1} & 0 & 0 & 0 & 0 & 0 & 0 & 0 & 0 & 0 \\ 0 & c_{b,1} & 0 & 0 & 0 & 0 & 0 & 0 & 0 & 0 \\ 0 & 0 & c_{b,1} & 0 & 0 & 0 & 0 & 0 & 0 & 0 \\ 0 & 0 & 0 & c_{t,1} & 0 & 0 & 0 & 0 & 0 & 0 \\ 0 & 0 & 0 & 0 & 0 & 0 & 0 & 0 & 0 & 0 \\ 0 & 0 & 0 & 0 & 0 & c_{b,2} & 0 & 0 & b_1 & 0 \\ 0 & 0 & 0 & 0 & 0 & 0 & c_{b,2} & 0 & b_2 & 0 \\ 0 & 0 & 0 & 0 & 0 & 0 & 0 & c_{b,2} & b_3 & 0 \\ 0 & 0 & 0 & 0 & 0 & b_1 & b_2 & b_3 & c_{t,2} & 0 \\ 0 & 0 & 0 & 0 & 0 & 0 & 0 & 0 & 0 & 0 \end{bmatrix}$$

$$\widetilde{K}(t)=\begin{bmatrix} k_{1,1} & 0 & 0 & 0 & 0 & k_{12} & 0 & 0 & 0 & 0 \\ 0 & k_{2,1} & 0 & 0 & 0 & 0 & k_{12} & 0 & 0 & 0 \\ 0 & 0 & k_{3,1} & 0 & 0 & 0 & 0 & k_{12} & 0 & 0 \\ 0 & 0 & 0 & k_{t,1} & 0 & 0 & 0 & 0 & 0 & 0 \\ 0 & 0 & 0 & 0 & k_{d1} & 0 & 0 & 0 & 0 & 0 \\ k_{12} & 0 & 0 & 0 & 0 & k_{1,2} & 0 & 0 & c_1 & 0 \\ 0 & k_{12} & 0 & 0 & 0 & 0 & k_{2,2} & 0 & c_2 & 0 \\ 0 & 0 & k_{12} & 0 & 0 & 0 & 0 & k_{3,2} & c_3 & 0 \\ 0 & 0 & 0 & 0 & 0 & c_1 & c_2 & c_3 & k_{t,2} & 0 \\ 0 & 0 & 0 & 0 & 0 & 0 & 0 & 0 & 0 & k_{d2} \end{bmatrix}$$

Where $k_{d,j}$ is the j^{th} damper stiffness given as $2\rho_l A_{d,j} g$ and $m_{d,j}$ is the mass of the j^{th} damper. Matrices for MBC transformation as follows

$$\Lambda_1=\begin{bmatrix} 1 & \cos\psi_1 & \sin\psi_1 & 0 & 0 \\ 1 & \cos\psi_2 & \sin\psi_2 & 0 & 0 \\ 1 & \cos\psi_3 & \sin\psi_3 & 0 & 0 \\ 0 & 0 & 0 & 1 & 0 \\ 0 & 0 & 0 & 0 & 1 \end{bmatrix} \qquad \Lambda_2=\begin{bmatrix} 0 & -\sin\psi_1 & -\cos\psi_1 & 0 & 0 \\ 0 & -\sin\psi_2 & -\cos\psi_2 & 0 & 0 \\ 0 & -\sin\psi_3 & -\cos\psi_3 & 0 & 0 \\ 0 & 0 & 0 & 0 & 0 \\ 0 & 0 & 0 & 0 & 0 \end{bmatrix}$$

$$\Lambda_1=\begin{bmatrix} 0 & -\cos\psi_1 & -\sin\psi_1 & 0 & 0 \\ 0 & -\cos\psi_2 & -\sin\psi_2 & 0 & 0 \\ 0 & -\cos\psi_3 & -\sin\psi_3 & 0 & 0 \\ 0 & 0 & 0 & 0 & 0 \\ 0 & 0 & 0 & 0 & 0 \end{bmatrix}$$

$$\Psi_1=\begin{bmatrix} \Lambda_1 & 0_{5\times5} \\ 0_{5\times5} & \Lambda_1 \end{bmatrix} \qquad \Psi_2=\begin{bmatrix} \Lambda_2 & 0_{5\times5} \\ 0_{5\times5} & \Lambda_2 \end{bmatrix} \qquad \Psi_3=\begin{bmatrix} \Lambda_3 & 0_{5\times5} \\ 0_{5\times5} & \Lambda_3 \end{bmatrix}$$